Radiocarbon age offsets between two surface dwelling planktonic foraminifera species during abrupt climate events in the SW Iberian margin

Blanca Ausín[1], Negar Haghipour[1], Lukas Wacker[1], Antje H. L. Voelker[2, 3], David Hodell[4], Clayton Magill[5], Nathan Looser[1], Stefano M. Bernasconi[1], Timothy I. Eglinton[1]

[1]Geological Institute, ETH Zürich, Zurich 8092 Switzerland

[2]Centre of Marine Sciences (CCMAR), Universidade do Algarve, Faro 8005-139 Portugal

[3]Instituto Português do Mar e da Atmosfera, 1495-006 Lisboa, Portugal

[4]Department of Earth Sciences, University of Cambridge, Cambridge CB2 3EQ United

[5]Lyell Centre, Heriot-Watt University, Edinburgh EH14 4AS United Kingdom

Kingdom

Corresponding author: Blanca Ausín (blanca.ausin@erdw.ethz.ch)

Key Points:

- Leaching of the outer shell is a powerful diagnostic for external subtle contamination and an effective tool to obtain more reliable radiocarbon dates.
- Co-occurring planktonic foraminifera species sampled across abrupt climatic events show radiocarbon age offsets of up to 1030 yr.
- Differential bioturbation coupled with species abundance changes is invoked to explain such temporal discrepancies.

Abstract

This study identifies temporal biases in the radiocarbon ages of the planktonic foraminifera species *Globigerina bulloides* and *Globigerinoides ruber* (white) in a sediment core from the SW Iberian margin (so-called 'Shackleton site'). Leaching of the outer shell and measurement of the radiocarbon content of both the leachate and leached sample enabled us to identify surface contamination of the tests and its impact on their ^{14}C ages. Incorporation of younger radiocarbon on the outer shell affected both species and had a larger impact down-core. Inter-species comparison of the ^{14}C ages of the leached samples reveal systematic offsets with ^{14}C ages for *G. ruber* being younger than *G. bulloides* ages during the last deglaciation and part of the Early and mid-Holocene. The greatest offsets (up to 1030 yr) were found during Heinrich Stadial 1 (HS1), the Younger Dryas (YD), and part of the Holocene. The potential factors differentially affecting these two planktonic species were assessed by complementary ^{14}C, oxygen and carbon isotopes, and species abundance determinations. The coupled effect of bioturbation with changes in the abundance of *G. ruber* is invoked to account for the large age offsets. Our results highlight that ^{14}C ages of planktonic foraminifera might be largely compromised even in settings characterized by high sediment accumulation rates. Thus, a careful assessment of potential temporal biases must be performed prior to using ^{14}C ages for paleoclimate investigations or radiocarbon calibrations (e.g. marine calibration curve Marine13 (Reimer et al., 2013)).

1 Introduction

For decades, fossil planktonic foraminifera have been a valuable source of paleoceanographic information, providing proxies for variations in ice-volume, sea level, salinity, temperature, and nutrients (e.g. Pearson, 2012). Since the discovery of the radiocarbon (^{14}C) dating technique in the late forties (Libby et al., 1949), radiocarbon age determination of planktonic foraminifera has become a cornerstone for paleoclimate investigations spanning the last 50,000 years. Most studies rely on this method to build chronostratigraphic frameworks for marine sediment sequences and constrain changes in thermohaline circulation by estimating radiocarbon ventilation ages. However, prior works have demonstrated that planktonic foraminifera ^{14}C ages might not always be a reliable indicator of their depositional ages due to numerous causes, as summarized by Mekik (2014). For instance, contamination trough radiocarbon addition by secondary calcite precipitation or adhesion of atmospheric carbon, which can go unnoticed during visual sample inspection under an optical microscope, can lead to large deviations in ^{14}C ages (Wacker et al., 2014; Wycech et al., 2016). Other possible causes of temporal biases include bioturbation along with differential dissolution and fragmentation (Barker et al., 2007, and references therein), differential bioturbation coupled with species abundance gradients (e.g. Bard et al., 1987b), transport and deposition of reworked specimens (Broecker et al., 2006), and distinct calcifying habitats (Lindsay et al., 2015). All these might differentially affect foraminifera species and their influence on foraminifera ^{14}C ages might be largely overlooked if, as in most paleo-investigations, only samples of one species are analyzed per sediment horizon. Thus, a more thorough assessment of the potential temporal biases between co-occurring foraminifera species is required prior conducting investigations primarily based on climate signals derived from foraminifera tests. Given age discrepancies might exceed the duration of abrupt climate events (> 1,000 yr) (Mekik, 2014), important questions arise in relation to the applicability of the latter approach in regions where marine sediments have a unique potential to unravel rapid climate and environmental changes.

In this regard, The so-called Shackleton sites, MD95-2042 and IODP Site U1385, on the SW Portuguese margin constitute benchmark cores for paleocenographic studies. For instance, Bard et al. (2004) produced a down-core sequence of *G. bulloides* ^{14}C ages in core MD95-2042, which was incorporated into IntCal09/Marine09 (Reimer et al., 2009) and subsequent updates (Reimer et al., 2013). This location has also emerged as one of the few regions in the world where direct correlation of marine signals with both Greenland and Antarctic ice-core signals are feasible (Shackleton et al., 2000), detailed chronostratigraphies have been developed (e.g. Bard et al., 1987a; Shackleton et al., 2004), and where ventilation and reservoir ages have been studied (Skinner & Shackleton, 2004; Skinner et al., 2014), all these based on ^{14}C ages of one species of planktonic foraminifera per sediment horizon.

Despite the importance attached to this location and prior works posing severe pitfalls to the latter approach, assessment of potential temporal biases trough ^{14}C determinations on paired species-specific samples has not yet been conducted. Consequently, potential temporal biases might have been disregarded in derived paleoclimate interpretations from this key study area. We aimed at identifying possible temporal biases in the ^{14}C ages of planktonic foraminifera species, analyzed in samples from a sediment core retrieved close to the location of IODP Site U1385, and assessing the potential causes for age deviations. To accomplish this, we investigated paired ^{14}C ages of two of the most commonly used planktonic foraminifera species: *Globigerina bulloides* and *Globigerinoides ruber* (white) and measured complementary oxygen (δ^{18}O) and carbon (δ^{13}C) isotopes, and species abundance data to elucidate possible reasons why radiocarbon ages may diverge for different foraminifera species from the same sample.

2 Study area

The SW Iberian margin (NE Atlantic Ocean) is a transitional region where the Portugal Current (PC), a branch of the North Atlantic Current, flows southward year-round (Fig. 1a) (Brambilla et al., 2008; Pérez et al., 2001). From October to March, the Iberian Poleward Current (IPC), a branch from the Azores Current, flows poleward along the W Portuguese margin (Haynes & Barton, 1990). This shift in the near-shore surface circulation is linked to the seasonal changes in the regional atmospheric circulation, which determine two well-differentiated oceanographic regimes. From March/April to September/October, prevailing northeasterly winds may induce Ekman transport offshore and subsequent upwelling of sub-surface waters. During the rest of the year, coastal downwelling occurs under prevailing southwesterly winds (Peliz et al., 2005). Upwelled sub-surface (100-500 m) waters consist in North Atlantic Central Water of either subtropical (NACWst; 100-250 m) or subpolar (NACWsp; 250-500 m) origin. The warmer and nutrient-poor NACWst overlies the colder, nutrient-richer NACWsp, which only upwells during strong upwelling events. Below the NACW, the denser Mediterranean Outflow Water (MOW) flows poleward between 500 and 1700 m. Below the intermediate waters, the Northeast Atlantic Deep Water (NEADW) flows southward (van Aken, 2000), along with varying contributions of the Upper Circumpolar Deep Water (UCDW), the Upper Labrador Sea Water (ULSW), and the Antarctic Bottom Water (AABW) (Jenkins et al., 2015).

3 Materials and Methods

We analysed down-core sediment samples from kasten core SHAK06–5K (37°34′N, 10°09′W, 2,646 m), recovered by RSS *James Cook* during the cruise JC089 in 2013 in the vicinity of the Shackleton Sites (*Hodell et al.*, 2014).

3.1. Radiocarbon determinations

The majority of the organic matter contained in the initial sediment was extracted with organic solvents following Ohkouchi et al. (2005) to use the organic fraction in a follow-up investigation. To assess the possible influence of this procedure on the foraminifera contained in the solvent-extracted residue, we also analysed five samples of *G. bulloides* tests selected from non-extracted sediments. Between 15-30 g of dry sediment were diluted in MiliQ® water and sonicated for only 15 seconds for disaggregation while avoiding shell fragmentation. The solution was then wet-sieved through 300 µm and 250 µm mesh sieves and thoroughly washed using a high-pressure stream of MiliQ® water. The resulting 250-300 µm size fraction was immediately dried at 60°C overnight, prior to collecting 45-100 well-preserved shells of *G. bulloides* or *G. ruber* from each sample. In some intervals, only 7-20 specimens of *G. ruber* were available, limiting the amount of measured carbon (Tables S1 and S2). Radiocarbon determinations ($^{14}C/^{12}C$) were performed with a gas ion source in a Mini Carbon Dating System (MICADAS) at the Laboratory of Ion Beam Physics, ETH Zürich with an automated method for acid digestion of carbonates whose sensitivity allows for less than10 µg of total carbon to be measured (*Wacker et al.*, 2013). The method is outlined as follows: vials (septa sealed 4.5 ml exetainers vials from Labco Limited, UK) containing the samples were purged for 10 min with a flow of 60 ml/min He to remove atmospheric CO_2. Later, samples were briefly leached by adding 100 µL of ultrapure HCl (0.02 M) with an automated syringe to remove possible surface contaminants. The CO_2 released from the leachate, referred to as “leachate” was transported by helium to a zeolite trap and automatically injected into the ion source to be measured for radiocarbon. The remaining sample, containing 12 µg C and referred to as “leached sample” was subsequently acidified by adding 100 µL of ultrapure H_3PO_4 (85%) that was heated to 60°C for at least 1 h. The released CO_2 was loaded in a second trap and injected into the ion source to be analyzed for radiocarbon (Wacker et al., 2014). Bard et al. (2015) showed that the $F^{14}C$ (fraction modern according to Reimer et al. (2004)) of leachates from sequential leaching of discrete samples converge towards a comparable value to that of the $F^{14}C$ of the leached sample (Bard et al., 2015). Thus, we propose differences < 5 % between the two values as an indication of near-complete removal of surface contaminants. Five replicates of *G. bulloide*s samples, referred to as “untreated”, were directly measured without leaching the outer shell to assess the necessity of this method. This gas ion source AMS system has a background $^{14}C/^{12}C$ value of $F^{14}C$ 0.0020+-0.0010 (50000 BP), determined on marble (IAEA-C1). Radiocarbon determinations were corrected for isotopic fractionation via $^{13}C/^{12}C$ isotopic ratios and are given in conventional radiocarbon ages. Radiocarbon ages and errors were not rounded to avoid artificial increments of age offsets and propagated errors.

3.2. Age-depth model

The age depth model for core SHAK06–5K is a depositional model (P_Sequence type) based on 41 ^{14}C ages of monospecific samples of *G. bulloides* (Table 1) built with the calibration package Oxcal (Bronk Ramsey, 2009). Conventional radiocarbon ages were calibrated to incorporate a static marine reservoir effect using Marine13 curve (Reimer et al., 2013). The resulting age-depth model spans the last 28,000 years.

3.3. Scanning Electron Microscope (SEM) imagery

Representative well-preserved specimens were selected from discrete intervals to assess surface preservation and possible early diagenetic overgrowth. Samples were graphite coated and SEM images were generated using a JEOL JSM-6390LA digital SEM with a W filament.

3.4. Oxygen and carbon stable isotope analyses

Oxygen and carbon stable isotope analyses were determined every 2 cm when possible. In total, 164 samples of *G. bulloides* and 140 samples of *G. ruber* were considered. Between 6 and 12 specimens of each species were measured with a Gas Bench II connected to a Delta V Plus isotope ratio mass spectrometer at the Stable Isotope Laboratory of Climate Geology, ETH Zurich (Breitenbach & Bernasconi, 2011). Calibration to the VPDB scale was accomplished using two in-house standards previously calibrated against the NBS-18 and NBS-19 international standards. The associated long-term standard deviation is < 0.07‰.

3.5. Species abundance

Representative aliquots of the 250-300 µm size fraction, containing at least 300 planktonic foraminifera shells, were obtained with a splitter. The relative and absolute abundances of *G. bulloides* and *G. ruber* were analysed in 33 samples spaced every 10 cm. Absolute abundances were calculated using the dry weight of the initial sieved sample.

4 Results

Radiocarbon ages of. *G. bulloides* samples from both extracted and non-extracted sediments show younger leachates (up to 2000 yr) compared to the corresponding leached samples (Fig. 2, Table 2). The leached samples from both types of sediments agree very well within their 1- σ error.

The 5 untreated samples are younger than the paired leached samples and older than the leachate (Fig. 3a). Age discrepancies among these three types of material measurements increase down-core.

Radiocarbon determinations generally reveal younger ages for the leachate in relation to the corresponding leached samples for both species (Fig. 3a-b, Table 3). Leached samples display a systematic aging down-core with few reversals of minimal magnitude. By contrast, ^{14}C ages of the leachate deviate from this trend, showing increasing variability down-core. While many of the age offsets between leached samples and paired leachates within the top 90 cm fall into their associated 1-σ uncertainty envelope, they show an apparent increase in magnitude down-core (up to 1595-1660 yr for both species at 260 cm, and up to 4015 yr for *G. bulloides* at the bottom of the core) (Fig. 3c, Table 3). Differences < 5 % between the $F^{14}C$ of leachates and corresponding leached samples indicate near-complete removal of surface contaminants for all the samples (Tables S1 and S2). Inter-species age differences of the leached sample reveal age offsets of up to 1030 yr, and only three of them overlap within their associated 1-σ uncertainty (Fig. 3d, Table 3). *G. bulloides* ages are generally older than *G. ruber* ones, a pattern that is reversed for two samples of the last glacial maximum, and within the top 20 cm of the core. The largest offsets coincide with the occurrence of three abrupt climate events: the Heinrich Stadial 1 (HS1), Younger Dryas (YD), and part of the Holocene (approximately 9-6 kyr). Limited material prevented some samples to be leached and were measured as untreated samples. Three of these *G. ruber* samples (280 cm, 270 cm, and a replicate of the latter) strongly deviate towards younger ages.

4.1. SEM imagery

Overall, tests of both species exhibit good preservation with minor overgrowth (i.e., secondary calcite) on the original base of the spines (Fig. S1). Such features are consistently observed in all samples, irrespective of their depth interval. Both, *G. bulloides* and *G. ruber* show variable amounts of coccoliths glued on the outer wall. Nevertheless, this feature does not affect all the samples nor all the specimens, and there is no relationship between the presence nor the amount of coccoliths and sample depth.

4.2. Isotopic composition of *G. bulloides* and *G. ruber*

Carbon isotopes of *G. bulloides* range between -0.4 and -1.8 ‰, and show higher values during the cold intervals associated to the HS2, HS1 and YD, and part of the Holocene (Fig. 4b). The $\delta^{13}C$ data of *G. ruber* vary between 1.4 and -0.4 ‰ and show relatively constant values for the first half of the record (340-170 cm) and an increasing trend towards more positive values thorough the Holocene. Oxygen isotopes of *G. bulloides* range between 0.1-3.0 ‰ and record short-term isotopic changes associated with HS2, HS1 and YD (Fig. 4c). The $\delta^{18}O$ data of *G. ruber* range between -0.1 and 2.2 ‰. This record shows a smoother profile than that of *G. bulloides* and lacks samples for part of HS1. Both isotopic curves are out-of-phase by at least 10 cm for most of the last deglaciation (70-140 cm). The oxygen isotopic difference between both species ($\Delta\delta^{18}O_{b-r}$) ranges from –0.3 ‰ to 1.7 ‰ and shows highest values during the HS2, HS1, and YD (Fig. 3c).

4.3. Variation in species abundances

Average absolute and relative abundances of *G. bulloides* are 6 specimens g^{-1} and 24%, respectively, and show large increases during the cold intervals HS2, HS1, and the YD (up to 25 specimens g^{-1} and 72%) (Fig. 4e). *G. ruber* shows average absolute and relative abundances of 1 specimens g^{-1} and 4%. This species is almost absent during HS2, HS1 and YD, and increases to up to 8 specimens g^{-1} and 13% during the late Holocene (top 30 cm).

5 Discussion

5.1. Contamination through secondary radiocarbon addition: the need for a leaching step

Age discrepancies between paired leached samples and leachates highlight the secondary addition of younger carbon and subsequent contamination on the outer shell (Fig. 3a and b, Table 3), as observed by previous authors when applying similar leaching steps (Bard et al., 2015). Such contamination was not introduced by using organic solvents for lipid extraction, as the leachates were always younger than corresponding leached samples, regardless of whether foraminifera come from solvent-extracted or non-extracted sediments (Fig. 2, Table 2). The magnitude of such age discrepancy does not always agree for both methods, but this can be explained by the varying and small amounts of C measured from the leachate (Table S1). Moreover, comparison of ^{14}C ages of leached samples from both types of sediments show negligible differences (Fig. 2). These results are in line with previous findings of Ohkouchi et al. (2005), who concluded that tests from solvent-extracted sediments can be reliably used for ^{14}C determinations. Additional influence of other sample preparation steps cannot be fully discarded. For instance, soaking of foraminifera during wet sieving can activate their reactive surface and enable adhesion of ambient carbon. However, we minimized the potential influence of this process by drying the samples in the oven right after sieving. Another possibility to consider is the influence of early diagenesis. Minor signs of secondary calcite precipitation are apparent by SEM imagery in all the tests (Fig. S1), regardless of sample depth and species. Diagenetic alteration of shells through $\sum CO_2$ exchange with pore waters with a younger ^{14}C signature might explain the negligible impact of secondary calcite precipitation on samples from the top 60 cm and the more variable and larger effect observed down-core (Fig. 3c). These results highlights the need of a leaching step to remove surface contaminants, especially for older samples, for which age biases can be greater than 1000 yr (Fig. 1a, Table 3).

Regarding the untreated samples of *G. ruber*, two large deviations toward younger-than-expected ages are also evident at the bottom of the core (Fig. 3b). Within single depth horizons of a core retrieved from the Portuguese margin, Löwemark and Grootes (2004) found large intra-species age discrepancies (up to 2590 years) when comparing sediments affected and unaffected by trace fossils indicating bioturbating organisms (e.g., *Zoophycos*). Because ichnofossils occur throughout the sediments of IODP Site U1385 (Rodríguez-Tovar & Dorador, 2014; Rodríguez-Tovar et al., 2015), they most certainly also affect the sediments of core SHAK06–5K. Their influence would imply that discrete samples from the same sediment horizon would consist of a mixture in different proportions of foraminifera tests from both bioturbated and non-bioturbated material. The excellent agreement between the two replicates of *G. ruber* samples from depth horizon 270 cm excludes bioturbation as the reason for such age deviations. Addition of younger secondary calcite might also explain these age deviations, although lack of material prevented further assessment.

5.2. Inter-species radiocarbon age differences

Assuming removal of the majority of external contamination by the leaching step (Table S1), secondary radiocarbon addition does not account for the ^{14}C age differences between the leached samples of the two species (Fig. 3d), and mechanism(s) differentially affecting foraminifera species must be sought to explain the systematic younger-than-*G. bulloides* ^{14}C ages for *G. ruber*. Ideally, such mechanism(s) should also explain changes in the magnitude of the observed age offsets with abrupt climate events. In the following, we discuss four possible mechanisms.

5.2.1. Contrasting calcifying habitats

Differences in calcifying depth and season of the two species might have also played a role in ^{14}C age discrepancies. Mollenhauer (1999) demonstrated that inter-species differences of 540 years are possible in upwelling settings, where deep, less-ventilated, "older" waters are upwelled to the surface. Currently in the study area, the average living depths (ALD) of *G. ruber* and *G. bulloides* are 58±6 and 102±21 m, respectively (Rebotim et al., 2017). While *G. ruber* is characteristic of winter hydrographic conditions, *G. bulloides* is more abundant during the upwelling season (i.e., summer) (Salgueiro et al., 2008). Figure 5 shows the natural radiocarbon content ($\Delta^{14}C$) depth profile from a station corresponding to the water column overlying the depositional area of the study site, extracted from the Global Ocean Data Analysis Project (GLODAP) (Key et al., 2004). Corresponding natural $\Delta^{14}C$ values for ALD of *G. ruber* and *G. bulloides* are -59 ‰ and ~ -65 ‰, respectively, equivalent to an age discrepancy of ~50 yr, which is insufficient to explain age offsets between species. As seasonality also impacts on the optimal conditions for *G. ruber* and *G. bulloides* proliferation, we calculated the winter and summer natural $\Delta^{14}C$ for the upper 500 m of the water column. We applied the linear relationship between natural $\Delta^{14}C$ and dissolved silicate for North Atlantic latitudes (equation (1)) proposed by Broecker et al. (1995), using summer and winter dissolved silicate estimates (García et al., 2014) averaged at 100 and 60 m water depth, respectively, from the 2013 World Ocean Atlas (WOA13).

$$\text{Natural } \Delta^{14}\text{C} = -60 - \text{dissolved silicate in } \mu\text{mol/kg} \quad (1)$$

Yet, the estimated seasonal difference in Δ^{14}C is minimal (-3.2 ‰) and negligible in relation to the large uncertainty derived from the silicate method (±15 ‰) (Rubin & Key, 2002).

However, it is still possible that the associated radiocarbon reservoirs (or at least one of them) varied in the past during HS1, YD, and part of the Holocene related to the large hydrographic changes that occurred during abrupt climate events in the study area (Voelker & de Abreu, 2011). This argument was put forward by Löwemark and Grootes (2004) to explain the large age discrepancy they found between *G. bulloides* and *G. ruber* during the YD on the Portuguese margin. In this regard, the incursion of intermediate, extremely ^{14}C–depleted waters characterized by high nutrient content has been suggested to reach latitudes as far as 60°N in the Atlantic during the abrupt cold intervals HS1 and YD (Pahnke et al., 2008; Rickaby & Elderfield, 2005; Thornalley et al., 2011). The authors pointed to Antarctic Intermediate Water (AAIW), which would have extended northward as a consequence of Atlantic Meridional Overturning Circulation (AMOC) weakening or collapse. Indeed, such drastic reductions of AMOC during HS1 and YD prevented the formation of new North Atlantic Deep Water (NADW) (McManus et al., 2004), which would have then been replaced by AAIW. However, the hypothesis of markedly different radiocarbon reservoirs affecting each of the species is not fully supported by other data. *G. ruber* δ^{13}C values give no clear indication of upwelling of nutrient-rich waters occurring during HS2 or YD, and lack of *G. ruber* during HS1 prevents further interpretation (Fig. 4b). More positive δ^{13}C values of *G. bulloides* rather suggest that upwelling had decreased at those times. Although less negative δ^{13}C values could also be the result of upwelling and subsequent nutrient consumption by primary producers, resulting in a ^{13}C-enrichment of surrounding waters, this scenario disagrees with previous studies. Estimates of export production by (Salgueiro et al., 2010) and of primary productivity and upwelling occurrence by (Incarbona et al., 2010) are best explained with the arrival of freshwater during HS1 and YD resulting in water column stratification, decreased upwelling and a large drop in productivity. Moreover, assuming that the general ecological preferences of each species remained constant during the last deglaciation, upwelling of AAIW would preferentially affect *G. bulloides.* Yet, radiocarbon ages corresponding to the δ^{18}O excursions of *G. bulloides* associated with HS2, HS1 and YD are in very good agreement with the established age ranges for these abrupt climate events (Fig. S2), which underpins the notion that *G. bulloides* ^{14}C ages are not, at least severely, biased in relation to their depositional ages. Additionally, we believe this mechanism fails to explain temporal discrepancies during the Holocene. Even though a relative increase of AAIW influence in higher northern latitudes can be recognized from neodymium isotope ratios (Pahnke et al., 2008), there is no evidence of a large reduction of AMOC at that time, which is believed to have been relatively strong during the Holocene (Gherardi et al., 2005; Thornalley et al., 2011). Although we cannot completely refute that the influence of water masses with distinct radiocarbon content (Δ^{14}C) contributed to the observed age offsets during HS1 and YD, an additional mechanism is needed to explain the smoothed δ^{18}O curve of *G. ruber* in relation to that of *G. bulloides* (Fig. 4c) a feature typical of bioturbated sediment (Bard et al., 1987a).

5.2.2. The Barker effect

The Barker effect (first proposed by Andree et al. (1984), Peng & Broecker (1984), Broecker et al. (1984), and Broecker et al. (2006) and coined by Broecker and Clark (2011), refers to the differential effect of partial dissolution and subsequent fragmentation of shells along with bioturbation on the ^{14}C ages of different species planktonic foraminifera (Barker et al., 2007; Broecker & Clark, 2011). Given that different species may dissolve at different rates, fragile and dissolution-prone species (i.e., *G. ruber*) will fragment in the sediment mixed layer more easily than more robust, dissolution-resistant species (i.e., *G. bulloides*) (Berger, 1968; 1970). This translates into shorter residence times in the sediment for *G. ruber* relative to *G. bulloides.* Consequently, the pool of non-fragmented shells of *G. ruber* at a given horizon will be biased towards younger specimens, because specimens that reside in the bioturbated layer for longer periods are more likely to be fragmented. As only well-preserved whole tests were picked for ^{14}C analyses, monospecific samples of *G. ruber* will be, on average, younger than *G. bulloides*.

This effect was invoked to account for age discrepancies among planktonic foraminifera species of up to several thousand years especially in cores characterized by low sediment accumulation rates (< 3 cm/kyr) (Barker et al., 2007; Broecker et al., 2006; Broecker & Clark, 2011; Peng & Broecker, 1984). The latter is an important factor to be taken into account since the lower the sedimentation rate, the longer the exposure time to the effect of bioturbation. High sedimentation rates of core SHAK06–5K only decrease to a minimum of 6 cm/kyr for the interval from 80 to 50 cm (Fig. 4a). However, the observed apparent increase in the inter-specific ^{14}C age offset is not exclusive to this horizon and visual inspection of nannofossils confirmed their excellent preservation thorough the Holocene.

Yet, highly productive settings may have favored acidification of underlying waters and pore waters through CO_2 release by respiration. Despite being part of a major upwelling system, total organic content in core SHAK06–5K and broader region (Baas et al., 1997; Magill et al., 2018) ranges from only 0.2 to 0.7 % for the whole studied period, suggesting that substantial dissolution by organic carbon oxidation is unlikely. Similarly, changes in the depth of the calcite lysocline are also assumed to have had a negligible effect, because the water depth of the core (2578 m) is located well above that level. Influence of more corrosive water masses could have promoted increased dissolution of *G. ruber*. However, incursion of southern sourced water-mass was mostly limited to glacial periods (Skinner & Shackleton, 2004), characterized by relatively high sedimentation rates. Therefore, we consider it is unlikely that the Barker effect had a major influence in the observed ^{14}C age discrepancies between foraminifera species.

5.2.3. Lateral and along-slope transport

Introduction of reworked specimens by advection and along-slope sedimentary processes could also contribute to radiocarbon age discrepancies, a mechanism proposed in cores from the Eastern Equatorial Pacific, the Mid-Atlantic Ridge, and the South China Sea (*Broecker et al.*, 2006). Addition of reworked calcareous nannofossils by lateral transport has been observed in the study area (Incarbona et al., 2010) and in core SHAK06–5K (Magill et al., 2018), especially during HS1. Simulated bottom velocities in the study area might locally exceed 10 cm/s, able to transport dense, 250-300 µm sized grains of foraminifera when locally reaching >40 cm/s (Hernández-Molina et al., 2011). To explain the observed older-than-*G. ruber* ages for *G. bulloides* by any of these mechanisms, transport and deposition of large numbers of reworked (old) *G. bulloides* would be necessary, along with preferential fragmentation of *G. ruber* during transport. This might be a feasible scenario, albeit it would imply that samples of *G. bulloides* are the ones affected by a temporal bias between biosynthesis and deposition. We thus discard this hypothesis based on: (i) the good agreement of *G. bulloides* $\delta^{18}O$ excursions during short-term climate changes and their associated established age ranges (Fig. S2) and (ii) the smoothed $\delta^{18}O$ curve of *G. ruber* that hardly resolves the major abrupt climate events occurred the last deglaciation (Fig. 4c). Such results suggest that *G. ruber,* rather than *G. bulloides,* accounts for the age offsets between the two species.

5.2.4. Differential bioturbation coupled with changes in species abundances

The joint effect of downward mixing of foraminifera due to bioturbation and changes in their abundance might promote ^{14}C offsets between species (Andree et al., 1984; Bard et al., 1987a; Broecker et al., 1999; Broecker et al., 1984; Peng & Broecker, 1984). Foraminifera will always be mixed from a horizon of high abundance to low abundance. Given an increase (decrease) in the abundance of a certain species in a sediment horizon, bioturbation is expected to down-mix (up-mix) some of these "young" ("old") foraminifera. As a result, the horizon underneath (above it) will be enriched in younger (older) specimens, leading to corresponding deviations in their expected ^{14}C ages. The clear aging trend with depth gives no indication of homogenization by bioturbation > 10 cm (Figs. 2a and b). However, the $\delta^{18}O$ record of *G. ruber* lags that of *G. bulloides* by 10 cm during the HS1, last deglaciation, and YD (Fig. 4d). This shift is more apparent when comparing samples at lower resolution (every 10 cm only) (Figure S3) and suggests a mixed layer depth equivalent to ≤ 10 cm. Similar out-of-phase relationships between species-specific isotopic records have previously been explained through this mechanism (Bard et al., 1987a; Bard et al., 1987b; Hutson, 1980). Löwemark and Grootes (2004) also invoked it to account for differences of 75-350 years between *G. bulloides* and *G. ruber* in a nearby core from the SW Portuguese margin. According to these authors, and given the large changes in the abundance of *G. bulloides* relative to those of *G. ruber* (Fig. 4e), a larger impact on the ^{14}C ages of the former species would be expected. This hypothesis is difficult to reconcile with the smoothed $\delta^{18}O$ curve of *G. ruber*. We would expect *G. ruber* to be the species more affected by differential bioturbation than *G. bulloides*. Indeed, and with the exception of the sample at 60 cm, each large increase in $\Delta\delta^{18}O$ is followed by a rise in *G. ruber* absolute abundance (Figs. 3c and d) that, despite their moderate magnitude, also follow periods of extremely low abundance or near absence. Our data is a faithful reproduction of previous mathematical simulations of Trauth (2013) and Bard et al. (1987a), who demonstrated the effects of bioturbation coupled with abundance changes in the oxygen isotopic record of a "warm" species (i.e., *G. ruber*) during deglaciation (see figure 4 in Bard et al., 1987a). Our results do not agree well with their model for the "cold" species (i.e., *G. bulloides*) because they are permanently present, and "authoctonous" specimens can make up for the radiocarbon addition from foraminifera belonging to adjacent sediment horizons.

6 Conclusions

Radiocarbon dates of paired monospecific samples of *G. bulloides* and *G. ruber* (white) were determined in marine sediments retrieved from the SW Iberian Margin. ^{14}C age differences of several thousands of years between paired leachates and leached samples indicate addition of younger radiocarbon in both species. This process is attributed to precipitation of younger secondary calcite by $\sum CO_2$ exchange with ^{14}C-rich pore waters and/or ambient carbon adhesion during sample sieving, thus having a more variable and greater impact down-core. Leaching of the outer shell has proven to be a powerful diagnostic for external contamination, and more importantly, a tool to obtain more reliable radiocarbon dates, especially when dealing with older samples (>10 kyr). Our findings underscore the need to properly leach foraminiferal samples prior to radiocarbon dating.

Inter-species age discrepancies of the leached samples ranged between 60 and 1030 years. *G. ruber* yielded younger ages than paired *G. bulloides* in the same sample throughout most of the record. Larger age discrepancies were found during HS1, YD, and part of the Holocene, and were attributed to the effects of bioturbation coupled with species abundance changes. This mechanism has a greater impact if the species in question has periods of absence (i.e., *G. ruber*) rather than greater abundance changes (i.e., *G. bulloides*) because the population of rarer species is more affected by the addition of asynchronous foraminifera compared to a more abundant species. This process alone appears to provide a satisfactory explanation for the observed age offsets, although additional influences such as past variations in the ^{14}C reservoirs of the respective calcifying habitats cannot be fully ruled out.

After a careful evaluation of potential ^{14}C age anomalies in these two species, we conclude that, unlike *G. ruber*, *G. bulloides* can be reliably used to develop foraminifera-based ^{14}C age chronostratigraphies and to assess ocean ventilation ages in the study area.

Author contribution

B.A. and T.I.E. planned this investigation. N.H. and L.W. assisted with radiocarbon analyses. N.L. assisted with SEM imagery. B.A. prepared the samples, analyzed the results and wrote the manuscript with contributions by all co-authors.

Acknowledgements and Data

We thank two anonymous reviewers for their valuable contribution to improve this manuscript. We would like to thank M. Jaggi for her assistance during isotope analyses. This study was supported by an ETH Zurich Postdoctoral Fellowship from the Swiss Federal Institute of Technology in Zurich (ETHZ) and the project 200021_175823 funded by Swiss National Science Foundation, both granted to B.A. A.H.L.V. acknowledges financial support from the Portuguese FCT through grants IF/01500/2014 and CCMAR (UID/Multi/04326/2013). The core for this study was collected during Cruise 089 aboard the RSS *James Cook* that was made possible with support from the UK Natural Environmental Research Council (NERC Grant NE/J00653X/1).

All original data used in this study, necessary to understand, evaluate and replicate this research is presented and available in tables within the main text and supporting information and it will be equally available in the public repository PANGAEA®.

References

Andree, M., Beer, J., Oeschger, H., Broecker, W., Mix, A., Ragano, N., . . . Wölfli, W. (1984). 14C measurements on foraminifera of deep sea core V28-238 and their preliminary interpretation. *Nuclear Instruments and Methods in Physics Research Section B: Beam*

Interactions with Materials and Atoms, 5(2), 340-345. doi:https://doi.org/10.1016/0168-583X(84)90539-1
Baas, J. H., Mienert, J., Abrantes, F., & Prins, M. A. (1997). Late Quaternary sedimentation on the Portuguese continental margin: climate-related processes and products. *Palaeogeography, Palaeoclimatology, Palaeoecology, 130*(1), 1-23. doi:https://doi.org/10.1016/S0031-0182(96)00135-6
Bard, E., Arnold, M., Duprat, J., Moyes, J., & Duplessy, J.-C. (1987a). Reconstruction of the last deglaciation: deconvolved records of δ18O profiles, micropaleontological variations and accelerator mass spectrometric14C dating. *Climate Dynamics, 1*(2), 101-112. doi:10.1007/bf01054479
Bard, E., Arnold, M., Duprat, J., Moyes, J., & Duplessy, J. C. (1987b). Bioturbation Effects on Abrupt Climatic Changes Recorded in Deep Sea Sediments. Correlation between δ18O Profiles and Accelerator 14C Dating. In W. H. Berger & L. D. Labeyrie (Eds.), *Abrupt Climatic Change: Evidence and Implications* (pp. 263-278). Dordrecht: Springer Netherlands.
Bard, E., Rostek, F., & Ménot-Combes, G. (2004). Radiocarbon calibration beyond 20,000 14C yr B.P. by means of planktonic foraminifera of the Iberian Margin. *Quaternary Research, 61*(2), 204-214. doi:https://doi.org/10.1016/j.yqres.2003.11.006
Bard, E., Tuna, T., Fagault, Y., Bonvalot, L., Wacker, L., Fahrni, S., & Synal, H. A. (2015). AixMICADAS, the accelerator mass spectrometer dedicated to C-14 recently installed in Aix-en-Provence, France. *Nucl Instrum Meth B, 361*, 80-86.
Barker, S., Broecker, W., Clark, E., & Hajdas, I. (2007). Radiocarbon age offsets of foraminifera resulting from differential dissolution and fragmentation within the sedimentary bioturbated zone. *Paleoceanography, 22*(2). doi:doi:10.1029/2006PA001354
Berger, W. H. (1968). Planktonic Foraminifera: selective solution and paleoclimatic interpretation. *Deep Sea Research and Oceanographic Abstracts, 15*(1), 31-43. doi:https://doi.org/10.1016/0011-7471(68)90027-2
Berger, W. H. (1970). Planktonic Foraminifera: Selective solution and the lysocline. *Marine Geology, 8*(2), 111-138. doi:https://doi.org/10.1016/0025-3227(70)90001-0
Brambilla, E., Talley, L. D., & Robbins, P. E. (2008). Subpolar Mode Water in the northeastern Atlantic: 2. Origin and transformation. *Journal of Geophysical Research: Oceans, 113*(C4). doi:doi:10.1029/2006JC004063
Breitenbach, S. F. M., & Bernasconi, S. M. (2011). Carbon and oxygen isotope analysis of small carbonate samples (20 to 100 µg) with a GasBench II preparation device. *Rapid Communications in Mass Spectrometry, 25*(13), 1910-1914. doi:doi:10.1002/rcm.5052
Broecker, W., Barker, S., Clark, E., Hajdas, I., & Bonani, G. (2006). Anomalous radiocarbon ages for foraminifera shells. *Paleoceanography, 21*(2). doi:doi:10.1029/2005PA001212
Broecker, W., & Clark, E. (2011). Radiocarbon-age differences among coexisting planktic foraminifera shells: The Barker Effect. *Paleoceanography, 26*(2). doi:doi:10.1029/2011PA002116
Broecker, W., Matsumoto, K., & Clark, E. (1999). Radiocarbon age differences between coexisting foraminiferal species. *Paleoceanography, 14*(4), 431-436. doi:doi:10.1029/1999PA900019
Broecker, W., Mix, A., Andree, M., & Oeschger, H. (1984). Radiocarbon measurements on coexisting benthic and planktic foraminifera shells: potential for reconstructing ocean ventilation times over the past 20 000 years. *Nuclear Instruments and Methods in Physics*

Research Section B: Beam Interactions with Materials and Atoms, 5(2), 331-339. doi:https://doi.org/10.1016/0168-583X(84)90538-X

Broecker, W. S., Sutherland, S., Smethie, W., Peng, T. H., & Ostlund, G. (1995). Oceanic radiocarbon: Separation of the natural and bomb components. *Global Biogeochemical Cycles, 9*(2), 263-288. doi:doi:10.1029/95GB00208

Bronk Ramsey, C. (2009). Bayesian Analysis of Radiocarbon Dates. *Radiocarbon, 51*(1), 337-360. doi:10.1017/S0033822200033865

García, H. E., Locarnini, R. A., Boyer, T. P., Antonov, J. I., Baranova, O. K., Zweng, M. M., . . . Johnson, D. R. (2014). World Ocean Atlas 2013, Volume 4: Dissolved Inorganic Nutrients (phosphate, nitrate, silicate). In S. Levitus & A. Mishonov (Eds.), *NOAA Atlas NESDIS 76* (pp. 25).

Gherardi, J. M., Labeyrie, L., McManus, J. F., Francois, R., Skinner, L. C., & Cortijo, E. (2005). Evidence from the Northeastern Atlantic basin for variability in the rate of the meridional overturning circulation through the last deglaciation. *Earth and Planetary Science Letters, 240*(3–4), 710-723. doi:http://dx.doi.org/10.1016/j.epsl.2005.09.061

Haynes, R., & Barton, E. D. (1990). A poleward flow along the Atlantic coast of the Iberian peninsula. *Journal of Geophysical Research: Oceans, 95*(C7), 11425-11441. doi:10.1029/JC095iC07p11425

Hernández-Molina, F. J., Serra, N., Stow, D. A. V., Llave, E., Ercilla, G., & Van Rooij, D. (2011). Along-slope oceanographic processes and sedimentary products around the Iberian margin. *Geo-Marine Letters, 31*, 315-341.

Hodell, D. A., Elderfield, H., Greaves, M., McCave, I. N., Skinner, L., Thomas, A., & White, N. (2014). *The JC089 scientific party, JC089 cruise report - IODP site survey of the Shackleton sites, SW iberian margin, British ocean data Centre. https://www.bodc.ac.uk/data/information_and_inventories/cruise_inventory/report/13392/*. Retrieved from

Hutson, W. H. (1980). Bioturbation of deep-sea sediments: oxygen isotopes and stratigraphic uncertainty. *Geology, 8*, 127-130.

Incarbona, A., Martrat, B., Di Stefano, E., Grimalt, J. O., Pelosi, N., Patti, B., & Tranchida, G. (2010). Primary productivity variability on the Atlantic Iberian Margin over the last 70,000 years: Evidence from coccolithophores and fossil organic compounds. *Paleoceanography, 25*(2), PA2218, doi:2210.1029/2008PA001709.

Jenkins, W. J., Smethie, W. M., Boyle, E. A., & Cutter, G. A. (2015). Water mass analysis for the U.S. GEOTRACES (GA03) North Atlantic sections. *Deep Sea Research Part II: Topical Studies in Oceanography, 116*, 6-20.

Key, R. M., Kozyr, A., Sabine, C. L., Lee, K., Wanninkhof, R., Bullister, J. L., . . . Peng, T. H. (2004). A global ocean carbon climatology: Results from Global Data Analysis Project (GLODAP). *Global Biogeochemical Cycles, 18*(4). doi:doi:10.1029/2004GB002247

Libby, W. F., Anderson, E. C., & Arnold, J. R. (1949). Age Determination by Radiocarbon Content: World-Wide Assay of Natural Radiocarbon. *Science, 109*, 227-228. doi:10.1126/science.109.2827.227

Lindsay, C. M., Lehman, S. J., Marchitto, T. M., & Ortiz, J. D. (2015). The surface expression of radiocarbon anomalies near Baja California during deglaciation. *Earth and Planetary Science Letters, 422*, 67-74. doi:https://doi.org/10.1016/j.epsl.2015.04.012

Löwemark, L., & Grootes, P. M. (2004). Large age differences between planktic foraminifers caused by abundance variations and Zoophycos bioturbation. *Paleoceanography, 19*(2). doi:doi:10.1029/2003PA000949

Magill, C. R., Ausín, B., Wenk, P., McIntyre, C., Skinner, L., Martínez-García, A., . . . Eglinton, T. I. (2018). Transient hydrodynamic effects influence organic carbon signatures in marine sediments. *Nature Communications, 9*(1), 4690. doi:10.1038/s41467-018-06973-w

McManus, J. F., Francois, R., Gherardi, J. M., Keigwin, L. D., & Brown-Leger, S. (2004). Collapse and rapid resumption of Atlantic meridional circulation linked to deglacial climate changes. *Nature, 428*, 834. doi:10.1038/nature02494

https://www.nature.com/articles/nature02494#supplementary-information

Mekik, F. (2014). Radiocarbon dating of planktonic foraminifer shells: A cautionary tale. *Paleoceanography, 29*(1), 13-29. doi:doi:10.1002/2013PA002532

Mollenhauer, G. (1999). *Einfluß von Bioturbation, Produktivität und Zirkulation auf 14C-Datierungen an planktonischen Foraminiferen.* (M.S.), University of Bremen.

Ohkouchi, N., Eglinton, T. I., Hughen, K. A., Roosen, E., & Keigwin, L. D. (2005). Radiocarbon Dating of Alkenones from Marine Sediments: III. Influence of Solvent Extraction Procedures on 14C Measurements of Foraminifera. *Radiocarbon, 47*(3), 425-432. doi:10.1017/S0033822200035207

Pahnke, K., Goldstein, S. L., & Hemming, S. R. (2008). Abrupt changes in Antarctic Intermediate Water circulation over the past 25,000 years. *Nature Geoscience, 1*, 870. doi:10.1038/ngeo360

https://www.nature.com/articles/ngeo360#supplementary-information

Pearson, P. N. (2012). Oxygen Isotopes in Foraminifera: Overview and Historical Review. *The Paleontological Society Papers, 18*, 1-38. doi:10.1017/S1089332600002539

Peliz, Á., Dubert, J., Santos, A. M. P., Oliveira, P. B., & Le Cann, B. (2005). Winter upper ocean circulation in the Western Iberian Basin—Fronts, Eddies and Poleward Flows: an overview. *Deep Sea Research Part I: Oceanographic Research Papers, 52*(4), 621-646. doi:http://dx.doi.org/10.1016/j.dsr.2004.11.005

Peng, T.-H., & Broecker, W. S. (1984). The impacts of bioturbation on the age difference between benthic and planktonic foraminifera in deep sea sediments. *Nuclear Instruments and Methods in Physics Research Section B: Beam Interactions with Materials and Atoms, 5*(2), 346-352. doi:https://doi.org/10.1016/0168-583X(84)90540-8

Pérez, F. F., Castro, C. G., Álvarez–Salgado, X. A., & Ríos, A. F. (2001). Coupling between the Iberian basin — scale circulation and the Portugal boundary current system: a chemical study. *Deep Sea Research Part I: Oceanographic Research Papers, 48*(6), 1519-1533. doi:https://doi.org/10.1016/S0967-0637(00)00101-1

Rebotim, A., Voelker, A. H. L., Jonkers, L., Waniek, J. J., Meggers, H., Schiebel, R., . . . Kucera, M. (2017). Factors controlling the depth habitat of planktonic foraminifera in the subtropical eastern North Atlantic. *Biogeosciences, 14*(4), 827-859. doi:10.5194/bg-14-827-2017

Reimer, P. J., Baillie, M. G. L., Bard, E., Bayliss, A., Beck, J. W., Blackwell, P. G., . . . Weyhenmeyer, C. E. (2009). IntCal09 and Marine09 radiocarbon age calibration curves, 0-50,000 years cal BP. *Radiocarbon, 51*, 1111-1150.

Reimer, P. J., Bard, E., Bayliss, A., Beck, J. W., Blackwell, P. G., Bronk Ramsey, C., . . . van der Plicht, J. (2013). IntCal13 and Marine13 Radiocarbon Age Calibration Curves 0-50,000 Years cal BP. Radiocarbon. *Radiocarbon, 55*.

Reimer, P. J., Brown, T. A., & Reimer, R. W. (2004). Discussion: Reporting and Calibration of Post-Bomb 14C Data. *Radiocarbon, 46*(3), 1299-1304. doi:10.1017/S0033822200033154

Rickaby, R. E. M., & Elderfield, H. (2005). Evidence from the high-latitude North Atlantic for variations in Antarctic Intermediate water flow during the last deglaciation. *Geochemistry, Geophysics, Geosystems, 6*(5). doi:doi:10.1029/2004GC000858

Rodríguez-Tovar, F. J., & Dorador, J. (2014). Ichnological analysis of Pleistocene sediments from the IODP Site U1385 “Shackleton Site” on the Iberian margin: Approaching paleoenvironmental conditions. *Palaeogeography, Palaeoclimatology, Palaeoecology, 409*, 24-32. doi:https://doi.org/10.1016/j.palaeo.2014.04.027

Rodríguez-Tovar, F. J., Dorador, J., Grunert, P., & Hodell, D. (2015). Deep-sea trace fossil and benthic foraminiferal assemblages across glacial Terminations 1, 2 and 4 at the “Shackleton Site” (IODP Expedition 339, Site U1385). *Global and Planetary Change, 133*, 359-370. doi:https://doi.org/10.1016/j.gloplacha.2015.05.003

Rubin, S. I., & Key, R. M. (2002). Separating natural and bomb-produced radiocarbon in the ocean: The potential alkalinity method. *Global Biogeochemical Cycles*, *16*(4), 52-51-52-19. doi:doi:10.1029/2001GB001432

Salgueiro, E., Voelker, A., Abrantes, F., Meggers, H., Pflaumann, U., Lončarić, N., . . . Wefer, G. (2008). Planktonic foraminifera from modern sediments reflect upwelling patterns off Iberia: Insights from a regional transfer function. *Marine Micropaleontology, 66*(3–4), 135-164. doi:http://dx.doi.org/10.1016/j.marmicro.2007.09.003

Salgueiro, E., Voelker, A. H. L., de Abreu, L., Abrantes, F., Meggers, H., & Wefer, G. (2010). Temperature and productivity changes off the western Iberian margin during the last 150 ky. *Quaternary Science Reviews, 29*(5–6), 680-695. doi:http://dx.doi.org/10.1016/j.quascirev.2009.11.013

Schlitzer, R. (2014). Ocean Data View, http://odv.awi.de (last access: 22 August 2018).

Shackleton, N. J., Fairbanks, R. G., Chiu, T.-c., & Parrenin, F. (2004). Absolute calibration of the Greenland time scale: implications for Antarctic time scales and for Δ14C. *Quaternary Science Reviews, 23*, 1513-1522. doi:http://dx.doi.org/10.1016/j.quascirev.2004.03.006

Shackleton, N. J., Hall, M. A., & Vincent, E. (2000). Phase relationships between millennial-scale events 64,000–24,000 years ago. *Paleoceanography, 15*, 565-569. doi:10.1029/2000pa000513

Skinner, L. C., & Shackleton, N. J. (2004). Rapid transient changes in northeast Atlantic deep water ventilation age across Termination I. *Paleoceanography, 19*(2). doi:doi:10.1029/2003PA000983

Skinner, L. C., Waelbroeck, C., Scrivner, A. E., & Fallon, S. J. (2014). Radiocarbon evidence for alternating northern and southern sources of ventilation of the deep Atlantic carbon pool during the last deglaciation. *Proceedings of the National Academy of Sciences, 111*(15), 5480-5484. doi:10.1073/pnas.1400668111

Thornalley, D. J. R., Barker, S., Broecker, W. S., Elderfield, H., & McCave, I. N. (2011). The Deglacial Evolution of North Atlantic Deep Convection. *Science, 331*(6014), 202-205. doi:10.1126/science.1196812

Trauth, M. H. (2013). TURBO2: A MATLAB simulation to study the effects of bioturbation on paleoceanographic time series. *Computers & Geosciences, 61*, 1-10. doi:https://doi.org/10.1016/j.cageo.2013.05.003

van Aken, H. M. (2000). The hydrography of the mid-latitude Northeast Atlantic Ocean: II: The intermediate water masses. *Deep Sea Research Part I: Oceanographic Research Papers, 47*(5), 789-824. doi:https://doi.org/10.1016/S0967-0637(99)00112-0

Voelker, A. H., & de Abreu, L. (2011). A Review of Abrupt Climate Change Events in the Northeastern Atlantic Ocean (Iberian Margin): Latitudinal, Longitudinal, and Vertical Gradients. In H. Rashid, L. Polyak, & E. Mosley-Thompson (Eds.), *Abrupt Climate Change: Mechanisms, Patterns, and Impacts*.

Wacker, L., Fahrni, S., & Moros, M. (2014). Advanced gas measurements of foraminifera: Removal and analysis of carbonate surface contamination *Ion Beam Physics, ETH Zurich Annual report*, 23.

Wacker, L., Lippold, J., Molnár, M., & Schulz, H. (2013). Towards radiocarbon dating of single foraminifera with a gas ion source. *Nuclear Instruments and Methods in Physics Research Section B: Beam Interactions with Materials and Atoms, 294*, 307-310. doi:https://doi.org/10.1016/j.nimb.2012.08.038

Wycech, J., Kelly, D. C., & Marcott, S. (2016). Effects of seafloor diagenesis on planktic foraminiferal radiocarbon ages. *Geology, 44*(7), 551-554. doi:10.1130/G37864.1

Figure 1. Location of core SHAK06–5K and age-depth model. Study area and surface circulation. PC: Portugal Current. IPC: Iberian Poleward Current. Modified from Voelker and de Abreu (2011).

Figure 2. Influence of the sample preparation method on radiocarbon ages. a) ^{14}C ages of the leachate (open circle) and the leached samples (dot) of *G. bulloides* picked from sediments extracted with organic solvents (light blue) and non-extracted sediments (dark blue). b) Age differences between paired leachates and leached samples from extracted (light blue) and non-extracted (dark blue) sediments, and between paired leached samples (black diamonds).

Figure 3. Radiocarbon ages and related offsets of planktonic foraminifera. (a) Radiocarbon ages of *G. bulloides* and (b) *G. ruber*. (c) ^{14}C-age discrepancies between the leached sample and the leachate of each species. (d) ^{14}C-age discrepancies between leached samples of both species calculated as *G. bulloides - G. ruber*. Open diamonds and dots in (c) and (d) indicate age offsets that fall within the 1-σ uncertainty envelope of the two ^{14}C dates, respectively. Grey bars mark periods or maximum age offsets, coinciding with the Heinrich Stadials (HS) 2 and 1, the Younger Dryas (YD), and part of the Early and mid-Holocene (E/M-H).

Figure 4. Oxygen isotopic records and abundances. (a) Sedimentation rate of core SHAK06–5K based on ^{14}C ages of leached samples of *G. bulloides*. (b) Carbon and (c) Oxygen isotope record of *G. bulloide*s and *G. ruber*. (d) Oxygen isotopic difference between *G. bulloides* and *G. ruber*. (e) Species absolute and relative abundances. Grey bars mark periods or maximum age offsets shown in figure 3, coinciding with the Heinrich Stadials (HS) 2 and 1, the Younger Dryas (YD), and part of the Early and mid-Holocene (E/M-H).

Figure 5. Modern estimated natural $\Delta^{14}C$ data at station ID15364 from GLODAP (*Key et al.*, 2004) corresponding to the overlying water column of SHAK06–5K core location. Data was plotted with ODV (*Schlitzer*, 2014).

Laboratory code	Depth (cm)	Radiocarbon age (14C yr BP)±1σ	Calendar age (yr cal. BP)±2σ
82182.2.1	0	790±150	414 ±112
82183.2.1	4	1010±150	591 ±92
72979.2.1	10	1250±70	815 ±72
82185.2.1	14	1450±70	1001 ±73
72981.2.1	20	1820±55	1367 ±60
72983.2.1	30	2300±50	1920 ±60
72985.2.1	40	3090±65	2879 ±82
75040.1.1	44	3620±75	3514 ±86
70397.1.1	48	3760±60	3702 ±82
75041.1.1	54	5300±80	5670 ±86
72987.2.1	60	7470±60	7923 ±68
72989.2.1	70	8740±70	9404 ±70
75042.1.1	76	9960±80	10925 ±128
72991.2.1	82	11050±85	12566 ±75
72993.2.1	90	11450±90	12913 ±108
70400.1.1	100	120100±110	13517 ±112
72995.2.1	110	12400±100	13909 ±117
72997.2.1	120	13250±95	15276 ±141
70403.1.1	130	136100±110	15875 ±149
72999.2.1	140	14100±100	16522 ±158
75043.1.1	146	14300±100	16864 ±161
73001.2.1	152	14900±100	17527 ±121
73002.2.1	160	14900±110	17742 ±113
73003.2.1	172	15350±110	18219 ±133
73005.2.1	180	15950±140	18791 ±122
75044.1.1	196	16650±120	19642 ±155
75016.1.1	200	17100±120	19989 ±143
75018.1.1	210	17300±120	20347 ±130
75020.1.1	220	17400±140	20679 ±162
75022.1.1	230	18600±180	21899 ±180
75024.1.1	240	18750±140	22241 ±131
70406.1.1	260	20000±180	23537 ±200

75028.1.1	270	20400±150	24012 ±156
75030.1.1	280	20700±150	24482 ±179
75048.1.1	284	201000±160	24781 ±215
75032.1.1	290	21300±160	25245 ±186
75033.1.1	300	22100±170	25936 ±125
75034.1.1	310	22600±180	26416 ±184
75036.1.1	320	23000±180	26974 ±210
75038.1.1	329	24100±200	27800 ±163

Table 1. Age model for core SHAK06–5K, based on monospecific samples of the planktonic foraminifera *Globigerina bulloides*. Convention radiocarbon ages and associated 1σ uncertainties have been rounded according to convention.

Table 2. Influence of the sample preparation method on radiocarbon ages. ^{14}C ages and associated 1-σ confidence level (68.2% probability), and corresponding age discrepancies, shown in figure 2. Age offsets that can be explained within the 1-σ confidence level of the associated dates are indicated in bold.

	G. bulloides from non-extracted sediments					*G. bulloides* from sediments extracted with organic solvents					*G. bulloides*- *G. bulloides*
	Leached sample		Leachate		Leached sample- Leachate	Leached sample		Leachate		Leached sample- Leach fraction	Leached Sample (Extracted sediment)-Leached sample (non-extracted sediment)
Depth (cm)	Lab code ETH-	14C age (yr)± 1 σ	Lab code ETH-	14C age (yr)± 1 σ	Age difference (yr)	Lab code ETH-	14C age (yr)±1 σ	Lab code ETH-	14C age (yr)± 1 σ	Age difference (yr)	Age difference (yr)
120	90559.1.1	12901±86	90559.2.1	12846±135	**55±160**	72997.2.1	13228±93	72997.1.1	12328±190	900±211	327±126
172	90557.1.1	15262±100	90557.2.1	13377±134	1885±167	73003.2.1	15346±115	73003.1.1	13730±202	1616±232	**84±152**
210	90555.1.1	17303±109	90555.2.1	16651±167	652±199	75018.1.1	17292±123	75018.2.1	15468±242	1824±271	**-11±164**
240	90553.1.1	18529±119	90553.2.1	16378±162	2151±201	75024.1.1	18735±134	75024.2.1	16214±256	2521±288	206±179
300	90552.1.1	22171±152	90552.2.1	21509±237	662±281	75033.1.1	22110±172	75033.2.1	20832±342	1278±382	**-61±229**

Table 3. Radiocarbon ages and associated 1-σ confidence level (68.2% probability), and corresponding age discrepancies. * Stands for untreated samples. Numbers in bold indicate age offsets that can be explained within the 1-σ confidence level of the associated dates.

	G. bulloides					*G. ruber*					*G. bulloides*- *G. ruber*	*G. bulloides*- *G. bulloides*
	Leached sample		Leachate		Leached sample- Leachate	Leached sample		Leachate		Leached sample-Leach fraction	Leached sample-Leached sample	Leached sample-Untreated sample
Depth (cm)	Lab code ETH-	^{14}C age (yr)± 1 σ	Lab code ETH-	^{14}C age (yr)± 1 σ	Age difference (yr)	Lab code ETH-	^{14}C age (yr)±1 σ	Lab code ETH-	^{14}C age (yr)± 1 σ	Age difference (yr)	Age difference (yr)	Age difference (yr)
0	*82182.2.1	788±151										
4	*82183.2.1	1012±153										
10	82184.2.1	1253±71	82184.1.1	1373±77	120±105	72980.2.1	1463±45	72980.1.1	1216±108	247±117	-210±84	

	*72979.1.1	1458±110										**-205±131**
14	*82185.2.1	1451±70										
20	72981.2.1	1820±55	72981.1.1	2078±124	-258±136	72982.2.1	1884±46	72982.1.1	1930±113	**-46±122**	**-64±72**	
30	72983.2.1	2301±47	72983.1.1	2229±120	**72±129**	72984.2.1	2471±75	72984.1.1	2349±123	**122±144**	-170±88	
40	72985.2.1	3087±64	72985.1.1	2927±117	160±133	*72986.1.1	2628±185					
44	75040.1.1	3619±74	75040.2.1	3823±124	-204±144							
48	70397.1.1	3762±62	70397.2.1	3848±122	**-86±137**	70399.1.1	3389±63	70399.2.1	3137±123	252±138	373±88	
54	75041.1.1	5295±80	75041.2.1	5343±122	**-48±146**							
60	72987.2.1	7470±63	72987.1.1	6556±149	914±162	72988.2.1	6705±60	72988.1.1	6964±207	-259±215	765±87	220±90
	*90560.1.1	7250±64										
70	72989.2.1	8744±69	72989.1.1	8731±156	**13±171**	72990.2.1	8482±89	72990.1.1	8261±157	221±180	262±113	
76	75042.1.1	9957±76	75042.2.1	9338±160	619±177							
82	72991.2.1	11056±84	72991.1.1	10351±180	706±199	72992.2.1	10204±75	72992.1.1	10130±175	**74±190**	852±113	
90	72993.2.1	11437±86	72993.1.1	11191±178	246±198	72994.2.1	10806±104	72994.1.1	10854±174	**-48±203**	631±135	
100	70400.1.1	12077±107	70400.2.1	11261±193	816±221	70402.1.1	11900±105	70402.2.1	11442±201	458±227	177±150	
110	72995.2.1	12385±103	72995.1.1	12413±187	-28±213	*72996.1.1	12318±210					
120	72997.2.1	13228±93	72997.1.1	12328±190	900±211	72998.2.1	12198±91	72998.1.1	12688±198	-490±218	1030±130	
130	70403.1.1	13615±109	70403.2.1	12794±204	821±231	70405.1.1	13193±109	70405.2.1	12905±304	**288±323**	422±154	336±140
	*90558.1.1	13279±88										
140	72999.2.1	14090±104	72999.1.1	13535±199	555±224	73000.2.1	13252±596	73000.1.1	11980±272	1272±655	838±605	
146	75043.1.1	14290±101	75043.2.1	13079±225	1211±247							
152	73001.2.1	14884±105	73001.1.1	14160±216	724±240							
160	73002.2.1	14924±108	73002.1.1	14334±210	590±236							
172	73003.2.1	15346±115	73003.1.1	13730±202	1616±232	*73004.1.1	14572±328					191±154
	*90556.1.1	15155±102										
180	73005.2.1	15977±138	73005.1.1	14560±207	1417±249	73006.2.1	15261±230	73006.1.1	15071±339	**190±410**	716±268	
190	73007.2.1	15916±206	73007.1.1	16179±247	**-263±322**	*73008.1.1	15513±260					
196	75044.1.1	16636±120	75044.2.1	15351±270	1285±295							
200	75016.1.1	17066±120	75016.2.1	16105±238	961±266	75017.1.1	16786±134	75017.2.1	16599±267	**187±299**	280±180	
210	75018.1.1	17292±123	75018.2.1	15468±242	1824±271	*75019.1.1	17064±161					
214	75045.1.1	17242±122	75045.2.1	16159±279	1083±304							

220	75020.1.1	17427±142	75020.2.1	16248±270	1179±305	75021.1.1	17511±137	75021.2.1	16493±260	1018±294	**-84±197**	
230	75022.1.1	18634±176	75022.2.1	17495±259	1139±313	*75023.1.1	18146±170					
234	75046.1.1	18305±130	75046.2.1	17318±278	987±307							
240	75024.1.1	18735±134	75024.2.1	16214±256	2521±289	75025.1.1	18301±177	75025.2.1	17803±280	498±331	435±222	1154±182
	*90554.1.1	17581±123										
250	75026.1.1	18726±150	75026.2.1	18314±288	412±325	75027.1.1	19231±141	75027.2.1	18481±289	750±322	-506±206	
260	70406.1.1	19979±181	70406.2.1	18387±301	1592±351	70408.1.1	19831±180	70408.2.1	18166±307	1665±356	**148±255**	
264	75047.1.1	19776±143	75047.2.1	17717±276	2059±311							
270	75028.1.1	20361±152	75028.2.1	17665±287	2696±325	*75029.1.1	18348 ±172					
270 r						*82186.2.1	18310±320					
280	75030.1.1	20684±155	75030.2.1	17045±257	3639±300	*75031.1.1	15814±166					
284	75048.1.1	20991±159	75048.2.1	18691±319	2300±356							
290	75032.1.1	213487±161	75032.2.1	20247±338	1100±374							
300	75033.1.1	22110±172	75033.2.1	20832±342	1278±383							
310	75034.1.1	22573±178	75034.2.1	20153±339	2420±383	*75035.1.1	21912±278					
314	75049.1.1	23133±189	75049.2.1	21020±484	2113±519							
320	75036.1.1	22984±185	75036.2.1	19376±305	3608±357	*75037.1.1	22763±286					1419±242
	*90551.1.1	21565±157										
329	75038.1.1	24126±203	75038.2.1	20116±317	4010±376	*75039.1.1	23166±329					

Figure 1.

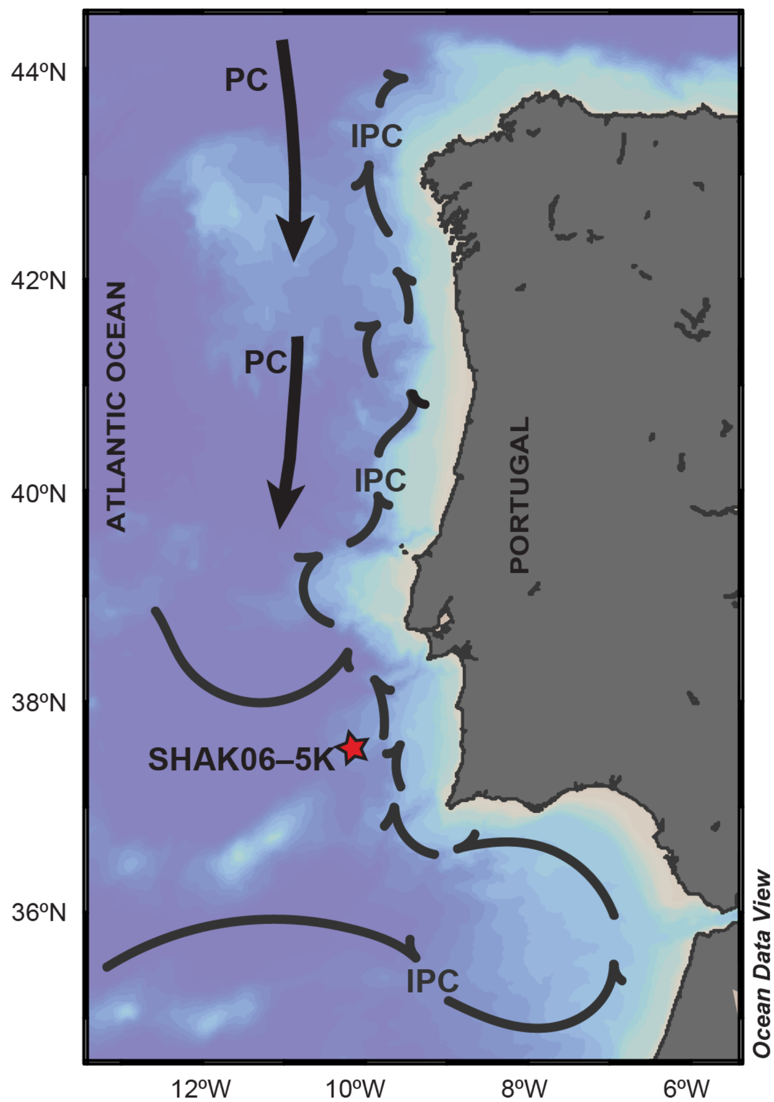

44ºN
42ºN
40ºN
38ºN
36ºN
12ºW
10ºW
8ºW
6ºW
PC
PC
IPC
IPC
IPC
ATLANTIC OCEAN
PORTUGAL
SHAK06–5K
Ocean Data View

Figure 2.

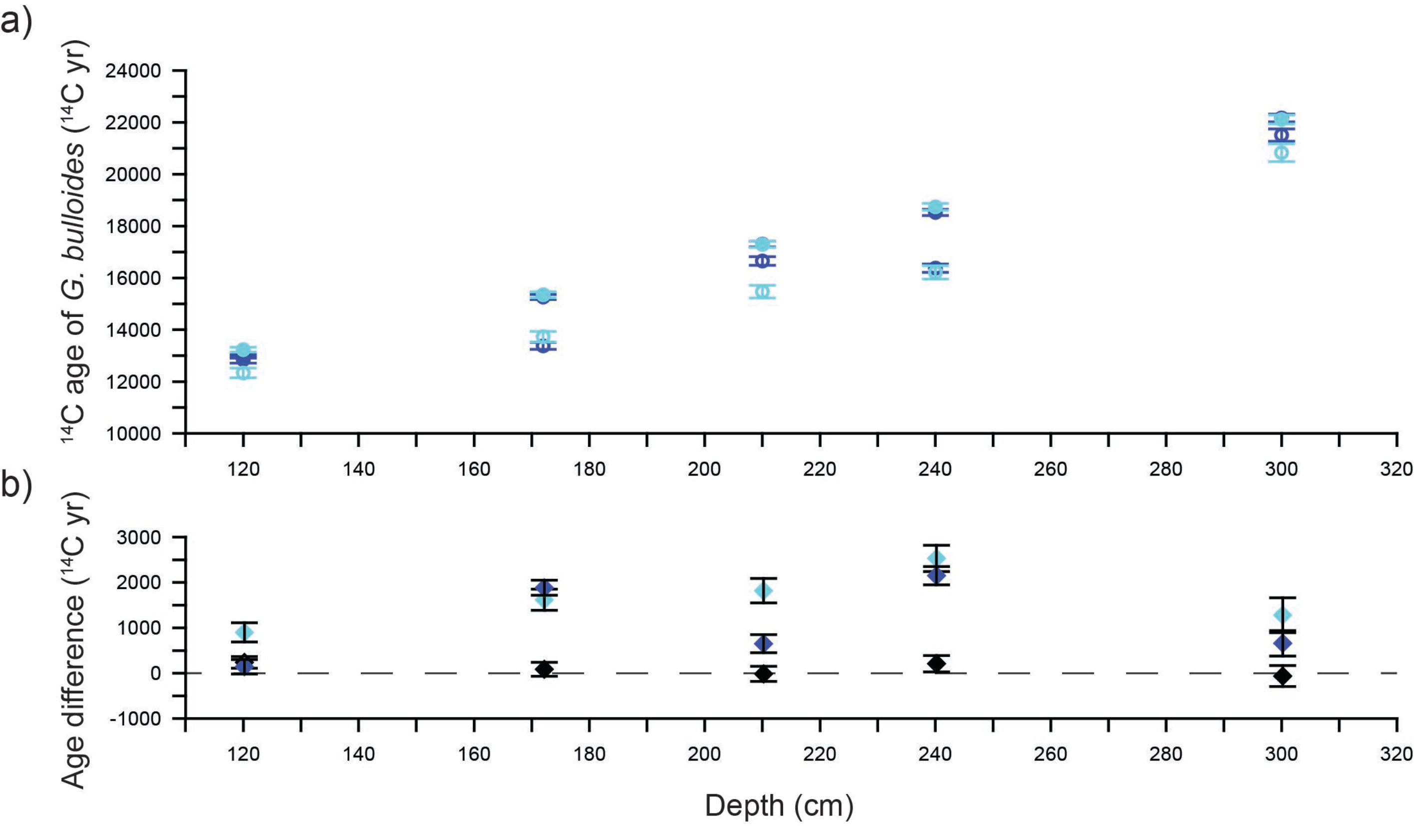
a)
b)
24000
22000
20000
18000
16000
14000
12000
10000
^{14}C age of *G. bulloides* (^{14}C yr)
120
140
160
180
200
220
240
260
280
300
320
3000
2000
1000
0
-1000
Age difference (^{14}C yr)
Depth (cm)

Figure 3.

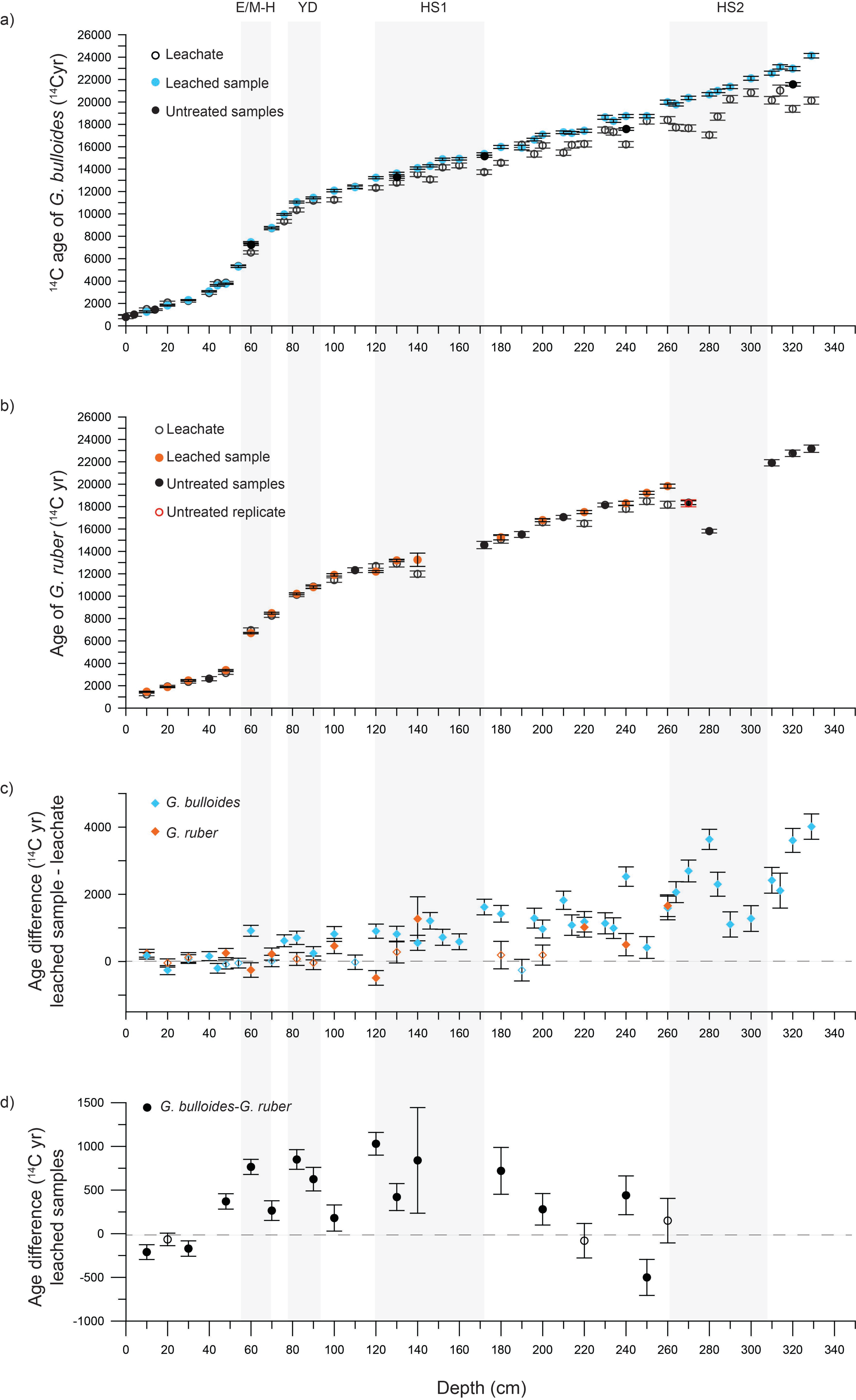

E/M-H
YD
HS1
HS2
a)
Leachate
Leached sample
Untreated samples
^{14}C age of G. bulloides (^{14}Cyr)
b)
Leachate
Leached sample
Untreated samples
Untreated replicate
Age of G. ruber (^{14}C yr)
c)
G. bulloides
G. ruber
Age difference (^{14}C yr) leached sample - leachate
d)
G. bulloides-G. ruber
Age difference (^{14}C yr) leached samples
Depth (cm)

Figure 4.

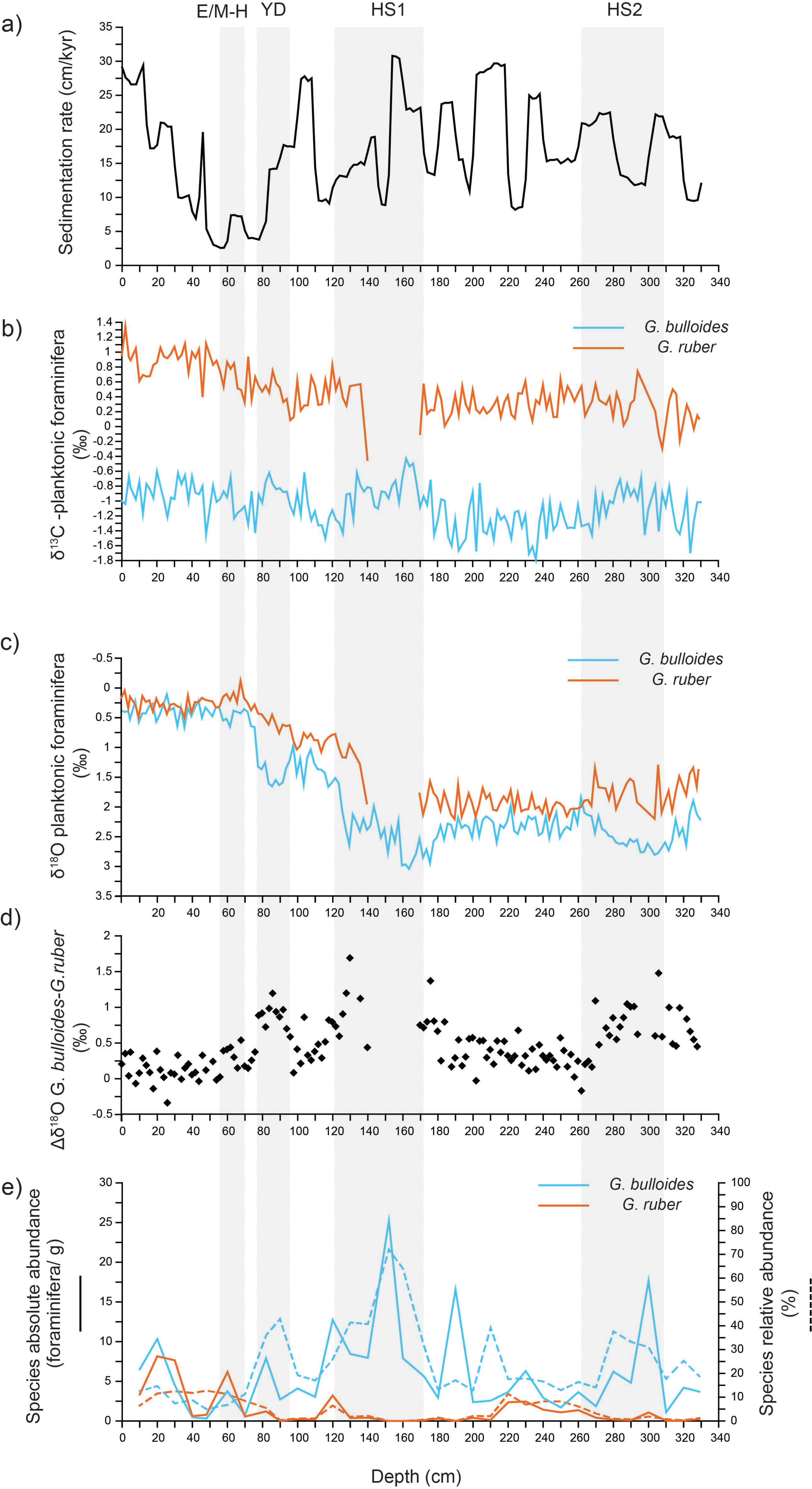

a)
E/M-H
YD
HS1
HS2
Sedimentation rate (cm/kyr)
b)
δ13C -planktonic foraminifera (‰)
G. bulloides
G. ruber
c)
δ18O planktonic foraminifera (‰)
G. bulloides
G. ruber
d)
Δδ18O G. bulloides-G.ruber (‰)
e)
Species absolute abundance (foraminifera/ g)
G. bulloides
G. ruber
Species relative abundance (%)
Depth (cm)

Figure 5.

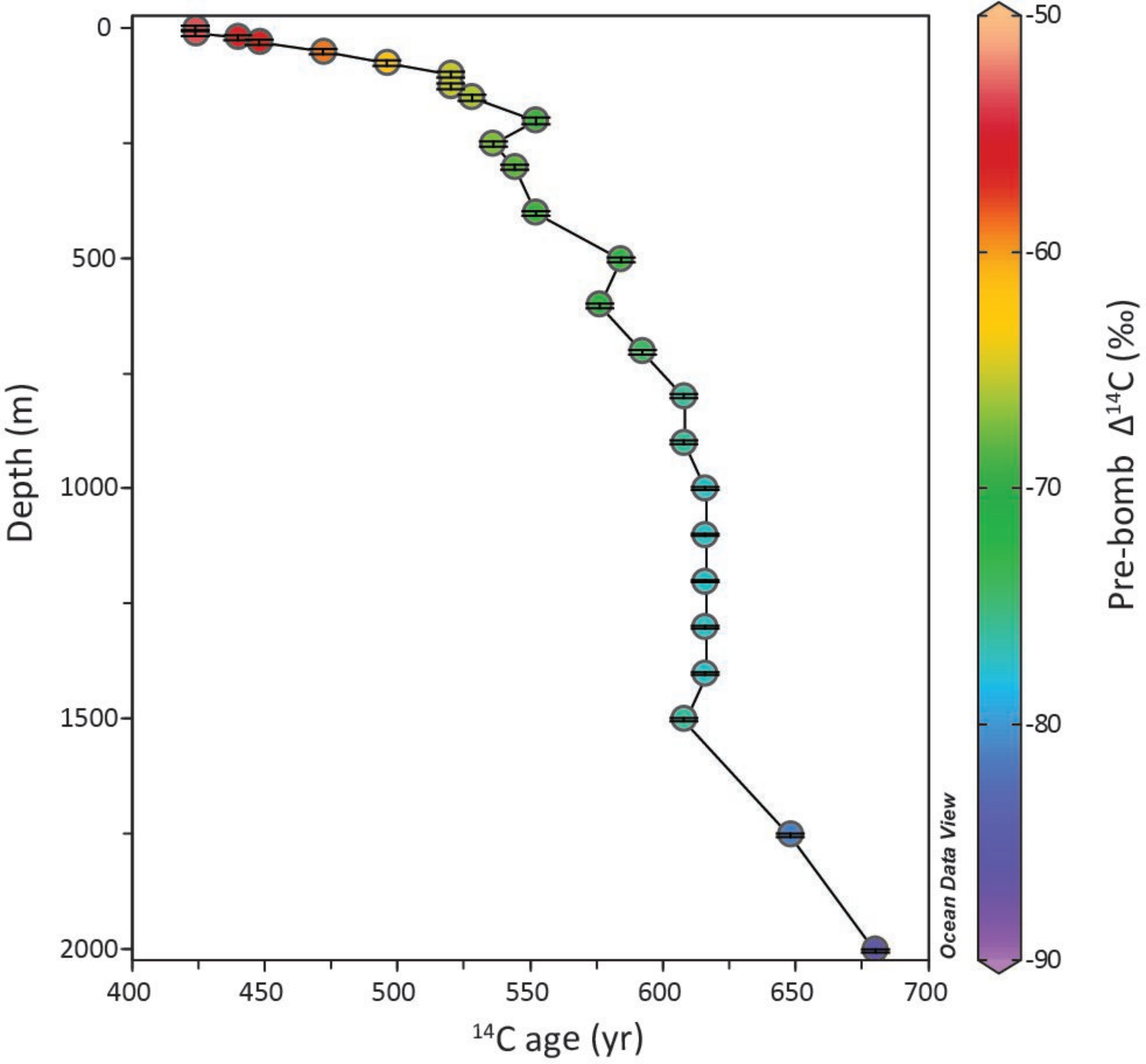

0
500
1000
1500
2000
Depth (m)
400
450
500
550
600
650
700
^{14}C age (yr)
Ocean Data View
-50
-60
-70
-80
-90
Pre-bomb $\Delta^{14}C$ (‰)